Biomaterials Advances 169 (2025) 214163

Contents lists available at ScienceDirect

Biomaterials Advances

journal homepage: www.journals.elsevier.com/materials-science-and-engineering-c

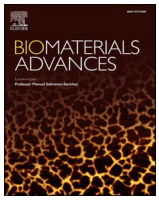

Abdominal PP meshes coated with functional core-sheath biodegradable nanofibers with anticoagulant and antibacterial properties

Malo Dufay [a], Maude Jimenez [a], Mathilde Casetta [a], Feng Chai [b], Nicolas Blanchemain [b], Mickael Maton [b], Frédéric Cazaux [a], Séverine Bellayer [a], Stéphanie Degoutin [a,*]

[a] Univ. Lille, CNRS, INRAE, Centrale Lille, UMR 8207 - UMET - Unité Matériaux et Transformations, F-59000 Lille, France
[b] Univ. Lille, Inserm, CHU Lille, U1008, Controlled Drug Delivery Systems and Biomaterials, F-59000 Lille, France

ARTICLE INFO

Keywords:
Coaxial electrospinning
Abdominal hernia treatment
Postoperative adhesions
Anticoagulant activity
Antibacterial activity

ABSTRACT

Abdominal hernia repair is a common surgical procedure, involving in most cases the use of textile meshes providing a mechanical barrier to consolidate the damaged surrounding tissues and prevent the resurgence of the hernia. However, in more than half cases postoperative complications such as adhesions and infections occur at the surface of the mesh, leading to chronic pain for the patient and requiring the removal of the implant. One of the most promising strategies to reduce the risk of postoperative adhesions and infections is to add a physical barrier between the mesh and the abdominal walls. In this study, we propose a strategy to develop functional hernia meshes possessing anticoagulant and antibacterial activities depending on the side of the implant. Two bioactive polymers were synthetized: a polysulfonate (poly(2-acrylamido-2-methylpropane sulfonic acid), PAMPS) one for anticoagulant activity and a polymer bearing ternary amines (poly((2-tert-butylamino) ethyl methacrylate), PTBAEMA) for antibacterial activity. These polymers were used to produce core-sheath nanofibers thanks to coaxial electrospinning with poly(ε-caprolactone) (PCL) as core and the bioactive polymer as sheath. The electrospinning parameters were optimized in order to obtain defect-free nanofibrous coatings onto the mesh with improved stability in water. The core-sheath structure was investigated as well as the presence of the functional groups at the surface. The *in vitro* cytocompatibility, anticoagulant activity and antibacterial activity were evaluated and highlighted the high potential of these coatings for the simultaneous prevention of postoperative adhesions and infections.

1. Introduction

The treatment of abdominal hernia represents the second most frequent surgical act with >20 million interventions/year in the world [1]. This disease occurs when a part of the bowel pushes through the abdominal wall because of the apparition of a non-natural cavity or to the relaxation of an already existing orifice. In rare cases, abdominal hernia does not require any surgery but mostly, the use of a mechanical barrier is necessary in order to avoid hernia recurrence. However, as for any operation, this surgery includes postoperative risks.

In terms of risks, the main one is postoperative adhesions which occur in more than half cases during the healing process after the intra-abdominal surgery [2]. Briefly, after injury due to the procedure, fibrin is naturally formed between the different layers of the intra-abdominal wall, as a step of the coagulation cascade. When the amount of fibrin is too high, fibrinolysis cannot occur within 5 days [3] and abnormal bands of fibrin are formed between these tissues and the peritoneum, leading to pain for the patient. The postoperative adhesions are often underestimated, because their consequences can be observed several months or even years after surgery, leading then to chronic pain, and are not always related to the postoperative adhesions. The follow-up of this major complication for both health and society is difficult as it is often handled by specialists other than the surgeon who handled the initial operation. Another risk mentioned in the literature is the infection of the parietal layer of the peritoneum after the surgery [4]. Indeed, infections can be hospital acquired infections which represent 7 to 8 % of total laparoscopy [5], or inflammatory response of the organism after implantation of meshes due to the presence of a foreign body [6]. These infections may occur at the surface of the mesh, but can also occur in an extended and deeper area, weeks to months after surgery. Depending on the severity of these infections, the explantation of the infected mesh is often unavoidable. Nowadays, the prevention of postoperative

* Corresponding author.
E-mail address: stephanie.degoutin@univ-lille.fr (S. Degoutin).

https://doi.org/10.1016/j.bioadv.2024.214163
Received 19 July 2024; Received in revised form 11 December 2024; Accepted 24 December 2024
Available online 3 January 2025

adhesions and infections has become the main objective for intra-abdominal implants improvement. Their consequences lead to adverse effects for the patient such as pain or longer convalescence period, as well as increased health expenses such as re-operation. To avoid these postoperative risks, several separate approaches have been considered [7].

Regarding ***adhesions***, the use of **pharmaceuticals agents**, **peritoneal instillation**, **hydrogels** and also **mechanical barrier** in addition to intra-peritoneal implant can be mentioned. Concerning the *pharmaceutical solutions*, the most studied are non-steroidal anti-inflammatory drugs, corticoids, fibrinolytic agents, and also antihistamines [8]. Heparin-like drugs are also considered as anticoagulant drugs to reduce the amount of fibrin formed during the coagulation cascade [9]. Some of these agents showed good results for the limitation of fibrin deposition, particularly on animal model. However, the fibrin formation process is also responsible for healing, and therefore for the reparation of traumatic area (inflammation and fibrin deposition). In consequence, these solutions lead frequently to supplementary infections (case of corticoids for example), to important hemorrhage risks, or also to important health expenditures due to the requirement of an additional surgical intervention to remove the implant. For *peritoneal instillation*, good results were obtained particularly for Adept® (4 % icodextrin solution, developed by Baxter BioSurgery), which allow a significant decrease of adhesions for patients for 4 to 8 weeks after laparoscopy [10]. However, its major issue is that the liquid is totally absorbed by the body within the 24 h after the surgery, whereas adhesion process occurs during the 3 to 5 days after this surgery, which leads to a re-injection requirement. For *hydrogels* and *mechanical barriers*, the deposition can be made directly by the surgeon onto the peritoneal meshes. For each case, a decrease of adhesions was observed with a limitation of the severity [11,12]. The main drawbacks of these techniques are their difficult handling and the necessity of an additional step for the surgeon to apply any of these prevention materials. Some commercial composite implants are also available, mainly based on synthetic meshes covered with hydrogel such as Parietene™ (polypropylene/collagen) or Sepramesh™ (polypropylene/carboxymethylcellulose) [8,13,14]. The clinical studies showed a good integration in the body, even for meshes coated on each side, and interesting prevention of post-operative adhesions, but this effect is also impacted by the inflammatory response [13].

Concerning ***infections*** prevention, several studies deal with the **release of therapeutic agents** [15–17]. Indeed, research was carried out on the use of antibiotics such as ciprofloxacin, ofloxacin or rifampicin directly impregnated or embedded into a hydrogel onto polypropylene (PP) [18] or polylactic acid (PLA) meshes or also on the use of metallic particles such as silver [17]. Furthermore, another strategy would be to functionalize the intra-peritoneal mesh with intrinsic *antibacterial polymers*. In this case, numerous families of polymers with antibacterial activity against Gram + and Gram − bacteria could be studied such as halogenic polymers, antimicrobial peptides, or polymers with quaternary amines for instance [19]. In the latter case, the antibacterial activity is related to the link between amines and the bacterial wall followed by its lysis, which leads to the release of all cytoplasmic compounds. Among all these polymers, it is possible to quote aromatic polymers as poly(4-vinylpyridine) [20], methacrylic polymers as 2-(dimethylamino)ethyl methacrylate [21], and also polyelectrolytes as poly(phenylethylene) [22]. The main drawback of these polymers is that the cytoplasmic compounds released after bacteria wall disaggregation are directly deposited on the polymer material and lead to its fouling [23]. In order to avoid this issue, some studies considered the use of quaternarisable amine polymers, which possess a ternary amine able to become a quaternary one, particularly during the contact with bacteria [24]. Interestingly, the ability of these polymers to transform ternary to quaternary amines allowed an antifouling effect by avoiding the deposition of bacteria compounds onto the polymer material.

In order to provide new properties to the meshes and develop “smart prostheses”, the latest promising strategies are to functionalize the surface with bioactive, biocompatible and biodegradable polymers [25]. To that purpose, numerous techniques can be employed as dip-coating, spray-coating, nebulization, electrospraying or electrospinning. The latter leads to the deposition of polymer nanofibers directly onto a collector, in this case covered by the mesh [25–28]. The nanofibrous coatings studied can be based on simple nanofibers or more complex structures: drug loaded nanofibers, nanoparticles carriers, multilayered nanofibrous constructs or even nanofibrous mats impregnated by hydrogels. The nanofibrous structure exhibits interesting properties such as high surface area and a material structure mimicking the extracellular matrix one. The main interest of the electrospinning technique is that the nanofibers cover the entire surface of the abdominal implants and not only the surface of the mesh fibers. This technique can be used with a wide range of polymers which are functional or easy to functionalize [29]. In a previous study, we developed polypropylene meshes (PPM) covered by poly(ε-caprolactone) (PCL) nanofibers further functionalized by a sulfonated monomer thanks to cold plasma induced graft-copolymerization [30]. These functionalized meshes exhibited high *in vitro* anticoagulant properties. Moreover, multicomponent structures can also be designed by electrospinning, in particular core-sheath nanofibers by using coaxial electrospinning. It would then be interesting to obtain nanofibers with a core based on biodegradable polymer and a sheath based on bioactive polymers possessing either antibacterial or antiadhesive properties, that could present a high contact surface with the surrounding tissues, and be deposited on each face of the implant in order to prevent simultaneously the two types of postoperative issues.

This study was therefore focused on the electrospinning of core-sheath nanofibers with biodegradable PCL as core and a sheath based on two different bioactive polymers: either poly(2-acrylamido-2-methylpropane sulfonic acid) (PAMPS) or poly[(2-tert-butylamino) ethyl methacrylate] (PTBAEMA). PAMPS was chosen for its anticoagulant activity, expected to play a role in the reduction of fibrin formation. PTBAEMA is a quaternarisable amine polymer, known for its antibacterial properties [24]. These nanofibers were directly deposited on each side of a polypropylene mesh (PPM) already used in the inguinal hernia treatment. Two series of biodegradable samples with either antibacterial or anticoagulant activity were then obtained. Finally, the *in vitro* cytocompatibility and bioactivity of each series was assessed: coagulation time for PCL/PAMPS nanofibers, or antibacterial effect against *E. coli* and *S. aureus* for PCL/PTBAEMA nanofibers.

2. Materials and methods

2.1. Materials

The solvents used for the synthesis were dioxane, ethanol (EtOH), and methyl ether ketone (MEK) and were provided by Acros Organics (Illkirch, France). Both monomers used for the syntheses, possessing carbon-carbon double bond which allowed radical reaction initiated by azobisisobutyronitrile (AIBN), were 2-acrylamido-2-methylpropane sulfonic acid (AMPS) and (2-tert-butylamino) ethyl methacrylate (TBAEMA), and were provided by Aldrich Chemicals (Saint Quentin Fallavier, France). Poly(ε-caprolactone) (PCL, 80,000 $g{\cdot}mol^{-1}$) was chosen for its biodegradable properties and was purchased from Aldrich chemicals (Saint Quentin Fallavier, France). The solvents used for the electrospinning solutions were formic (95–97 %) and acetic acid (>99.8 %) provided by Honeywell (Seelze, Germany), dimethylformamide (DMF), dichloromethane (DCM), ethylacetate and acetonitrile purchased from Aldrich chemicals (Saint Quentin Fallavier, France). All solvents and reagents were used as received. Polypropylene meshes (PPM) (porosity of 73 ± 1 %, thickness of 0.25 ± 0.13 mm, and mass per unit area of 32 ± 4 g/m2) were kindly provided by Cousin Surgery (Wervicq-Sud, France) and were washed by soxhlet extraction (ethanol, water and ethanol successively).

2.2. Methods

2.2.1. Synthesis of the bioactive polymers PAMPS and PTBAEMA

AMPS was polymerized in order to obtain the homopolymer PAMPS. Briefly, 8.52 g of AMPS were dissolved in 43 mL of a water/dioxane (2/8) mixture in a 100 mL round-bottom flask under stirring. The pH of the solution was fixed around the pKa of AMPS (~1.5) by adding a few drops of NaOH 0.1 mol·L^{-1}. The flask was then covered by a septum under nitrogen flow. The mixture was finally heated at 60 °C. In parallel, AIBN was dissolved in 2 mL of water/dioxane (2/8) mixture and then added dropwise into the system. The 24 h reaction time started after the addition of all AIBN. At the end of the reaction, the crude was precipitated in 1 L of acetone and the solid was dried overnight under vacuum at 60 °C. The viscosimetric molecular weight M_v of PAMPS was calculated using intrinsic viscosities values determined thanks to an Ubbelohde no. 531-10/l viscosimeter with capillaries of 0.63 mm diameter and using a 5 N NaCl solution as solvent at 25 °C. Mark-Houwink parameters of PAMPS in this solvent were described in the literature as $\alpha = 0.80$ and $K = 2.11 \times 10^{-5}$ g/dL [31].

TBAEMA was polymerized in PTBAEMA (Fig. 8) following the protocol described by Sosna et al. [32]. In a 500 mL round-bottom flask covered by a septum, 90 mL of TBAEMA were mixed with 180 mL of EtOH at 70 °C under nitrogen flow. Then, 0.745 g of AIBN were dissolved in 20 mL of MEK and added dropwise to the system under stirring. After 72 h of reaction, the crude was precipitated in 1 L of distilled water, then filtrated under Büchner, and finally dried overnight under vacuum at 70 °C. The molecular weight M_W of synthesized PTBAEMA was determined by steric exclusion chromatography (SEC) using DMF as solvent. The apparatus was composed by an Agilent 1260-series HPLC system equipped with two PL gel 5 μm Mixed-D columns in series and a 1260 refractive index detector (RID).

2.2.2. Simple electrospinning

Before proceeding to coaxial electrospinning, the electrospinning of each bioactive polymer was carried out in order to determine optimal electrospinning parameters for each solution. In this sense, PAMPS solution was obtained by dissolving dried synthetized PAMPS (20 wt%) in a mixture formic acid/acetic acid (5/5) (AFA 5:5). Electrospinning of PAMPS solution was carried out at a tip-to-collector distance of 20 cm, with varying feeding rates and voltages, and the environmental parameters (relative humidity and temperature) were measured during the experiments. For PTBAEMA solutions (25 wt%), three mixtures of solvent were used: DCM/acetonitrile 5:5 (DAc), DMF/Ethyl acetate 5:5 (DMFAe), or AFA 5:5. Electrospinning of these solutions was optimized in terms of process, solution and environmental parameters. For comparison with core-sheath nanofibers obtained by coaxial electrospinning, mixtures of PCL and bioactive polymer (PAMPS or PTBAEMA) in AFA were also electrospun in similar conditions.

2.2.3. Coaxial electrospinning

In order to obtain bioactive core-sheath nanofibers by coaxial electrospinning, two separate electrospinning solutions were prepared. The inner PCL solution was obtained following the process established in a previous study [30]. Succinctly, PCL was dissolved in AFA 5:5 at a concentration of 12 wt%. The outer solution, based on either PAMPS or PTBAEMA previously synthesized, was prepared in the optimal conditions (solvent, concentration) determined from simple electrospinning. The inner and outer solutions were then injected through a pipe and a needle (21 gauge) and the flows were varied in order to observe their effect on the core-sheath structure. Nanofibers were deposited onto each face of PPM directly fixed onto a rotating collector (200 rpm).

2.2.4. Scanning electron microscopy (SEM), energy-dispersive X-ray spectroscopy (EDX) and transmission electron microscopy (TEM)

This work was carried out on the electron microscopy facility of the Advanced Characterization Platform of the Chevreul Institute. The morphology and diameters of the nanofibers were analyzed using a SEM Flexsem 1000 Hitachi with an accelerating voltage of 5 kV and an emission current of 10 μA. EDX analysis was carried out with the same apparatus in the same conditions. All the samples were carbon coated with a 20 nm layer. The average diameter of the nanofibers was evaluated by ImageJ software, taking into account the metallization thickness and on the basis of 100 measurements.

The core-sheath structure of coaxial nanofibers was observed and compared to classical nanofibers thanks to a FEI Tecnai G2-20 twin TEM, equipped by a LaB6 filament operate with an accelerated tension of 200 kV.

2.2.5. Thermogravimetric analysis (TGA)

The synthesized PAMPS and PTBAEMA were characterized by TGA, using a TA Q50 apparatus (TA Instruments, France) in order to confirm the removal of any residual solvent. Experiments were carried out in the 30–600 °C temperature range with a heating rate of 10 °C/min in a 90 % O_2–10% N_2 atmosphere.

2.2.6. Fourier transform infrared spectroscopy (FTIR)

Infrared analysis was carried out in attenuated total reflection (ATR) using a spectrum Two spectrometer provided by Perkin Elmer (Villebon-sur-Yvette, France). An accumulation of 16 scans was used for each spectrum with a resolution of 4 cm^{-1}. Infrared analysis was used to study the polymerization of AMPS. Concerning core-sheath nanofibers, the technique did not allow to distinguish the different layers of these membranes because of the penetration depth of 0.5 mm of FTIR beam. The results can be found in supplementary data.

2.2.7. Water contact angle (WCA)

Surface wettability and hydrophilicity, was characterized by studying the contact angle of a water drop deposited on samples and analyzed thanks to a Minitec Krüss DSA 100 goniometer (Krüss, Hamburg, Allemagne).

2.2.8. In vitro biological assays

Prior to biological assays, all samples were sterilized by gamma irradiation (40 kGy). SEM picture of the structure of the membranes after gamma irradiation is shown in supplementary data (fig. S3). All *in vitro* assays were carried out in triplicate.

2.2.8.1. In vitro cell viability by direct contact. Sterile disks of 11 mm diameter (n = 3) were placed in a 48-well TCPS plate. Cells (NIH/3T3 fibroblasts) were then seeded (4000 cells·cm^{-2}) directly onto disks and cultured during 3 to 6 days at 37 °C without any change of the cellular medium (Eagle GIBCO αMEM (ThermoFisher Scientific, Waltham, USA), supplemented by 50 μg/mL of gentamicin (Panpharma, Boulogne-Billancourt, France), 250 μg/mL of Fungizone® GIBCO (ThermoFisher Scientific, Waltham, USA) and 10 % of Fetal Bovine Serum (Eurobio, Les Ulis, France). After this incubation time, the medium was extracted and replaced by a solution composed by 180 μL of complete cellular medium and 20 μL of Alamar Blue® during 2 h into an incubator protected from light. The medium was analyzed by fluorometry at an emitted wavelength of 590 nm after an excitation at 560 nm thanks, to a Twinkle TMLB 970 fluorimeter. Each sample was compared to the control TCPS (Tissue Culture PolyStyrene) (cellular viability of 100 %). Obtained results were normalized thanks to a negative control.

2.2.8.2. In vitro coagulation assays. In accordance with ISO standard 10993-4, two disks of each sample (11 mm diameter) were immersed in healthy complete blood collected in citrate tube. Samples immersed in blood were incubated at 37 °C for 30 min, stirred at 80 rpm and centrifuged at 2500*g* at 15 °C for 15 min in order to separate red blood cells and poor platelet plasma (PPP). Three tests were then carried out: the *activated partial thromboplastin time* (*APTT*) in which 50 μL of PPP

were incubated at 37 °C for 1 min, mixed with 50 µL of TriniCLOT® aPTT HS, Tcoag® (TCA) reactive, incubated for 5 min and finally the coagulation time was measured after addition of 100 µL of $CaCl_2$ (0.025 mol·mL^{-1}); the *prothrombin time* (*PT*) in which 100 µL of PPP were incubated at 37 °C for 2 min, mixed with 200 µL of NEOPLATINE® provided by Diagnostica Stago, Inc. (Parsipanny, USA) (incubated at 37 °C for 10 min) and then the coagulation time was measured; and finally the *anti-Xa* which follows the provider HYPHEN BioMed (Neuville-sur-Oise, France) protocol (BIOPHEN™ Heparin Anti-Xa — 2 stages Heparin assay).

2.2.8.3. In vitro microbiological assays. PP-PCL/PTBAEMA coaxial/mixture nanofibers were tested in microbiological assays (with PP-PCL/PAMPS coaxial/mixture nanofibers as control). Microbiological assays were carried out following the kill-time method, which means that the number of unities forming bacterial colony (ufc) found on samples compared to the time of seeding was measured. Several contact times were evaluated from 30 min to 24 h. During these assays, analysis was realized in triplicate. Sterilized disk samples of 11 mm of diameter of each series were put into contact with bacterial strain Gram +: *Staphylococcus aureus* CIP224 and Gram −: *Escherichia coli* K12. Strains were sub cultured in a brain heart broth culture before dispersion onto a Muller-Hinton solid culture medium (agar) for 24 h, in order to be in their growth period before contact with samples and avoid the lag phase of bacteria. After these 24 h, 10 mL of Ringer cysteine (RC) liquid were added in order to ensure the osmotic equilibrium with bacteria. After this adding, the number of bacteria was about 10^9, requiring a dilution by 3 to reduce the bacteria amount. After dilution, 200 µL of bacteria solution were added in a 24-well plate (untreated polystyrene) containing samples and then incubated in an oven at 37 °C for 30 min to 24 h. Samples were then transferred in glass tubes containing 2 mL of Phosphate Buffered Saline (PBS), subjected to ultrasonic treatment for 1 min and finally vortexed for 30 s in order to solubilize bacteria. In order to measure the bacteria amount, each solution was finally diluted by 3 in RC liquid to facilitate the bacteria count.

2.2.8.4. Statistical analysis. All the results are expressed in value ± standard deviation. *In vitro* cellular viability and coagulation results of PCL/PAMPS membranes were analyzed by ANOVA and a significant difference was described for $p < 0.05$.

3. Results

3.1. Development of core-sheath nanofibers coated visceral implants based on PAMPS

3.1.1. Synthesis of PAMPS

In this study, PAMPS was synthesized using classical radical polymerization using AIBN initiator in a mixture of water/dioxane 2:8. The polymerization was followed by ^{1}H NMR (Fig. 1). The disappearance of peaks attributed to vinyl protons of monomer at 6.2 and 5.7 ppm attested the formation of polymer without any residual monomer at the end of the reaction. The absence of peak related to dioxane showed good removal of the solvent, as confirmed by TGA (Fig. S2A). The kinetics were followed and demonstrated a total conversion of the monomer after 24 h.

FTIR-ATR spectrum of PAMPS (Supplementary data, Fig. S1) highlighted the disappearance of the peak at 1612 cm^{-1} compared to the spectrum of AMPS. This peak was attributed to C═C insaturation of monomer, which proves again that the radical polymerization was achieved. The absence of this peak also demonstrates that there is no residual monomer at the end of the reaction, which supports the results obtained by ^{1}H NMR. The viscosimetric molecular weight M_v of PAMPS was estimated at 200,000 g•mol^{-1}.

3.2. Electrospinning

3.2.1. Simple electrospinning of PAMPS

After purification by successive thermal treatments and crushing, PAMPS was solubilized at a concentration of 20 wt% in AFA 5/5 (solvent mixture already used for PCL electrospinning in our previous study [30]) and electrospun. Defect-free nanofibers were obtained with a diameter of 290 ± 68 nm with an applied voltage of 24 kV and a flow rate of 0.1 mL•h^{-1}. For an applied voltage or a flow rate higher or lower, the jet was destabilized and prevented the deposition of nanofibers. This can be explained by the presence of repulsive forces inside PAMPS chains, thanks to their polyelectrolyte nature, which cause a jet instability. It was also impossible to obtain defect-free nanofibers for concentrations lower than 20 wt%. It is important to note that the PAMPS nanofibers were also completely soluble in water.

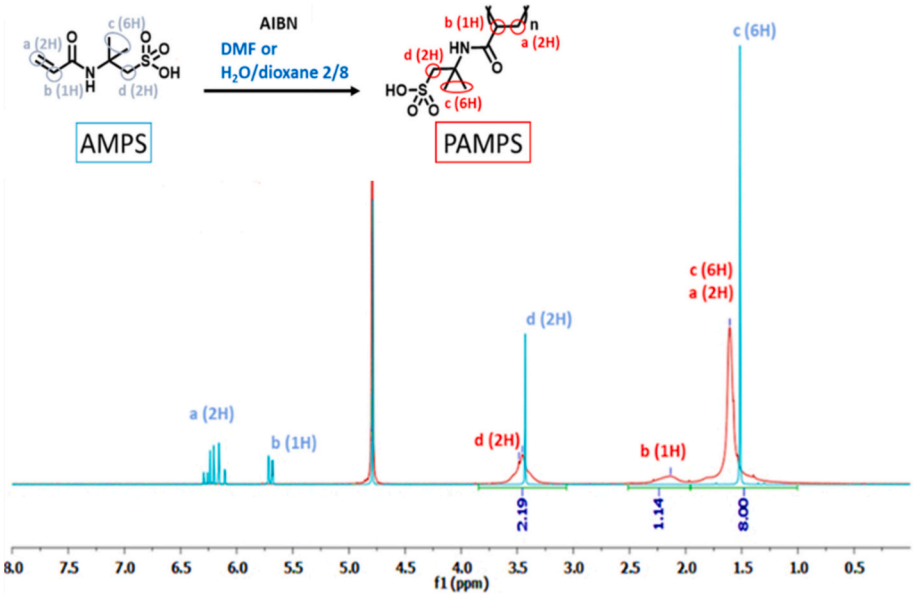

Fig. 1. ^{1}H NMR spectra of AMPS (blue) and PAMPS (red) after 24 h of reaction. (For interpretation of the references to color in this figure legend, the reader is referred to the web version of this article.)

3.2.2. Coaxial electrospinning of PCL/PAMPS

Core/sheath nanofibers were prepared by electrospinning of a 12 wt % PCL solution in AFA 5/5 as core solution and 20 wt% PAMPS solution in AFA 5/5 as sheath solution onto a PP mesh. In coaxial electrospinning, one of the most important parameters affecting the structure and morphology of nanofibers is the flow rate of each solution. In this sense, the studied couples of flow rates are presented in Table 1 and the morphology observed by SEM of the electrospun nanofibers obtained are presented in Fig. 2.

It is important to note that the electrospinning parameters differ for each condition in order to obtain defect-free nanofibers. Indeed, for C1 conditions, a high applied potential was necessary (23 kV) and the Taylor cone was difficult to stabilize. For C3 conditions, a high applied voltage was also necessary (26 kV) which led to an instability of the jet, and therefore to the formation of droplets during the process. The obtained membrane exhibited some solvent spots due to these droplets, nevertheless the morphology of these nanofibers seems homogeneous with an average diameter of 292 ± 107 nm. C4 conditions allowed the formation of nanofibers at a voltage of 15 kV and with a higher amount of PAMPS expected in the coaxial nanofibers (higher flow rate for PAMPS than for PCL). However, the nanofibers obtained in these conditions exhibit a higher average diameter (514 ± 112 nm), which makes them hardly analyzed by TEM. Finally, C2 conditions using a voltage of 22 kV led to the formation of smooth and defect-free nanofibers with an average diameter of 209 ± 64 nm. Therefore, only C1 and C3 conditions were excluded.

In order to compare the physicochemical properties of core/sheath nanofibers and monolithic nanofibers, a solution composed by a mixture of 6 wt% of PCL and 10 % of PAMPS in AFA 5/5 has also been electrospun at a flow rate of 0.3 $mL \bullet h^{-1}$ (similar conditions to C2, but with monolithic structure due to simple electrospinning). The obtained nanofibers exhibited an average diameter of 220 ± 96 nm with a defect-free structure. TEM analysis was then carried out to observe any core-sheath structure and images are presented in Fig. 3.

As expected, TEM image of the nanofiber obtained from a mixture of PCL and PAMPS did not exhibit any core-sheath structure (Fig. 3C. Moreover, TEM observation allowed to observe a very thin sheath thickness for nanofibers obtained from conditions C4 (Fig. 3B). In contrast, electrospun nanofibers from conditions C2 exhibited a core-sheath structure confirmed by a contrast difference (Fig. 3A). Therefore, C4 conditions were excluded and PCL/PAMPS mixture ones were used for further characterization in order to compare the two types of structure (core/sheath *vs.* monolithic ones).

Water contact angle assays were performed for membranes obtained from both process conditions. Results showed some differences between the two membranes. Indeed, water contact angle on core-sheath nanofibers obtained from conditions C2 was 56 ± 2° against 64 ± 4° for nanofibers obtained from mixture conditions. As expected, higher hydrophilicity was observed for nanofibers obtained from coaxial electrospinning. Indeed, PCL is hydrophobic (WCA around 138° for pure PCL nanofibers [30]) whereas PAMPS is hydrophilic (WCA around 52° for pure PAMPS nanofibers). Therefore, as core-sheath nanofibers possess a higher amount of PAMPS at their surface compare to monolithic ones, they exhibit a higher hydrophilic character than the nanofibers obtained from a mixture of PCL and PAMPS.

Table 1
Flow rates used for coaxial electrospinning of core-sheath PCL/PAMPS nanofibers in AFA 5/5.

	12 wt% PCL (core)	20 wt% PAMPS (sheath)
C1	0.5 $mL \bullet h^{-1}$	0.1 $mL \bullet h^{-1}$
C2	0.2 $mL \bullet h^{-1}$	0.1 $mL \bullet h^{-1}$
C3	0.1 $mL \bullet h^{-1}$	0.1 $mL \bullet h^{-1}$
C4	0.1 $mL \bullet h^{-1}$	0.2 $mL \bullet h^{-1}$

3.2.3. Enhancement of aqueous stability of PCL/PAMPS nanofibers

As biological assays require nanofibers to be stable in aqueous medium, samples obtained in conditions C2 were immersed in water for 30 min and their morphology was then observed by SEM (Fig. 4A).

Surprisingly, membranes kept their nanofibrous structure with an average diameter similar to nanofibers before immersion (209 ± 64 nm before immersion against 202 ± 77 nm after immersion for C2 conditions). However, EDX analysis showed a significant decrease of the sulfur amount after immersion (Fig. 5). Indeed, each membrane exhibits a ratio S/O of 20/80 before immersion against 3/97 after immersion. Our hypothesis was that the sheath of PAMPS was nearly totally dissolved in water, leaving only the core of PCL which swelled in contact with water, explaining the similar diameters of the nanofibers before and after immersion in water.

In order to enhance the stability of core/sheath nanofibers in water, a thermal treatment for 1 h at 70 °C was considered. As the melting point of PCL is around 60 °C, a thermal treatment at a higher temperature could lead to a melting of the core, which could partially diffuse into the sheath of PAMPS. The Tg of PAMPS is 55 °C, determined by Differential Scanning Calorimetry. This study was followed by EDX in order to quantify the amount of sulfur in core-sheath and monolithic membranes before and after immersion in water (Fig. 5).

These results showed that, in the case of core-sheath nanofibers without thermal treatment, the amount of sulfur decreased after immersion in water, while no significant decrease of the ratio S/O was observed after the thermal treatment at 70 °C. In comparison, for the mixture PCL/PAMPS, the thermal treatment did not allow to maintain the sulfur amount after immersion in water. Thus, our hypothesis is that the core of PCL melted and diffused partially through the sheath of PAMPS which led to multiple physical contact areas between PCL and PAMPS, preserving the sulfonate functions at the surface and avoiding the dissolution of the sheath of PAMPS in aqueous medium.

TEM analyses were also carried out on thermal treated (70 °C, 1 h) PCL/PAMPS core-sheath nanofibers obtained in C2 conditions (Fig. 4B). Results showed that the core-sheath morphology is maintained after thermal treatment and argue once more for the hypothesis of partial diffusion of the PCL core through the PAMPS shell without deformation of the nanofibrous structure.

Thus, the presented analyses allowed to conclude on the core/sheath structure in C2 conditions and a conservation of the nanofibrous structure after immersion in aqueous medium, indicating that the thermally treated membranes are suitable for biological evaluation assays.

3.3. Development of core-sheath nanofibers coated visceral implants based on PTBAEMA

3.3.1. Synthesis of PTBAEMA

PTBAEMA was synthetized in similar conditions as PAMPS ones in ethanol at a temperature of 70 °C for 72 h under inert atmosphere and using AIBN as initiator. The polymer was extracted after synthesis by precipitation/filtration and a thermal extraction of solvent under vacuum at 50 °C. The synthesis was followed by ^{1}H NMR (Fig. 6) and the conversion of monomer to polymer was easily observed thanks to the disappearance of broad peaks, particularly between 2.05 and 2.25 ppm. The absence of peak related to ethanol showed good removal of the solvent, as confirmed by TGA (Fig. S2B). A kinetic follow-up study showed that a reaction time of 72 h was necessary to achieve a total conversion of monomer to polymer.

The molecular weight M_W of synthesized PTBAEMA was determined by SEC at around 95,000 $g \bullet mol^{-1}$. The M_n was also measured at 40,000 $g \bullet mol^{-1}$ giving a polydispersity index (PDI) of ~2.4.

3.3.2. Electrospinning

3.3.2.1. Simple electrospinning of PTBAEMA. As for PAMPS, PTBAEMA

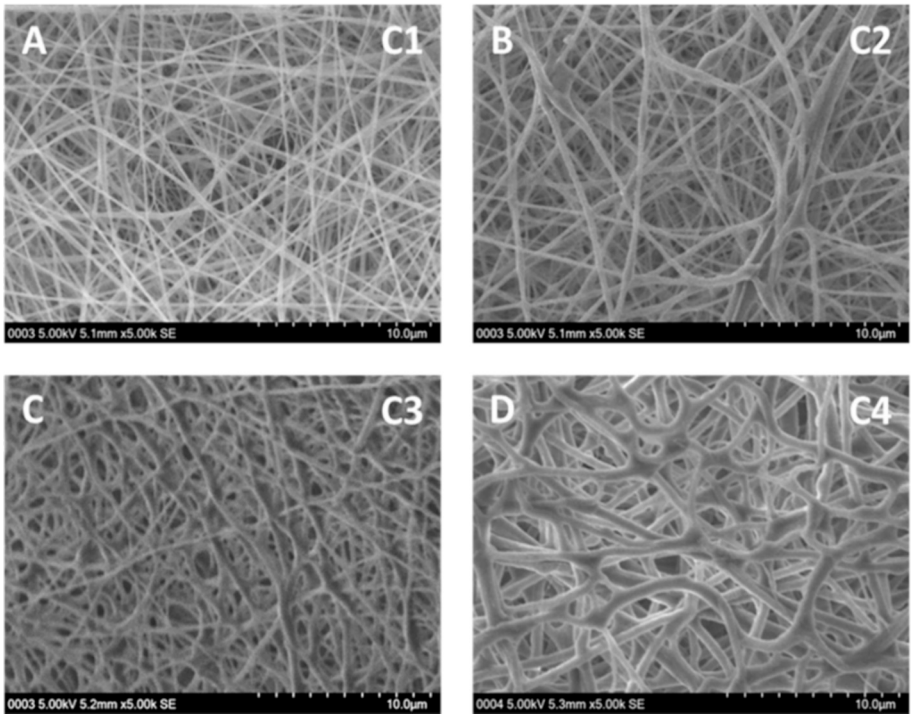

Fig. 2. SEM images of core-sheath nanofibers obtained from an inner solution of 12 wt% PCL in AFA 5/5 and an outer solution of 20 wt% PAMPS in AFA 5/5 in conditions: (A) C1 (147 ± 38 nm); (B) C2 (209 ± 64 nm); (C) C3 (292 ± 107) nm; (D) C4 (514 ± 112) nm.

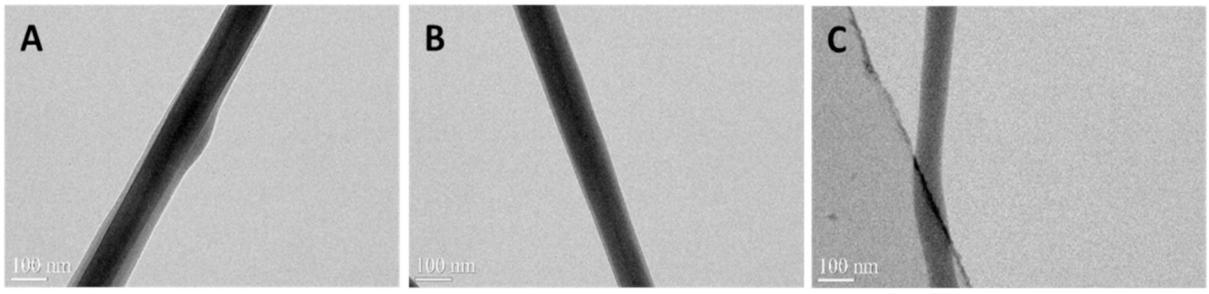

Fig. 3. TEM images of PCL/PAMPS nanofibers obtained: A) from coaxial electrospinning in C2 conditions; B) from coaxial electrospinning in C4 conditions and C) from simple electrospinning in PCL/PAMPS mixture conditions.

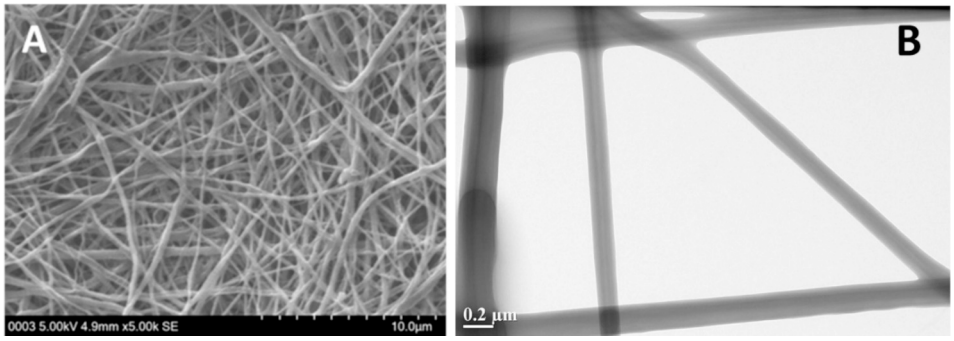

Fig. 4. PCL/PAMPS core-sheath nanofibers obtained in conditions C2: (A) SEM image after immersion in water for 30 min and (B) TEM image after a thermal post-treatment at 70 °C for 1 h.

was first electrospun alone in order to determine the optimal solution parameters. Three mixtures of solvent were used: acetic/formic acid (AFA 5/5), DCM/acetonitrile (Dac 5/5) and DMF/ethyl acetate (DMFAe 5/5). PTBAEMA was fast solubilized in each mixture (around 3 h) up to a concentration of 25 wt%. Its electrospinning at different concentrations from 14 to 25 wt% was then optimized. First, the flow rate and tip-to-collector distance were fixed at 0.5 $mL \bullet h^{-1}$ and 20 cm respectively. The morphology of each membrane observed by SEM is reported in Fig. 7.

These results showed that for concentrations of 14 wt% with AFA 5/5

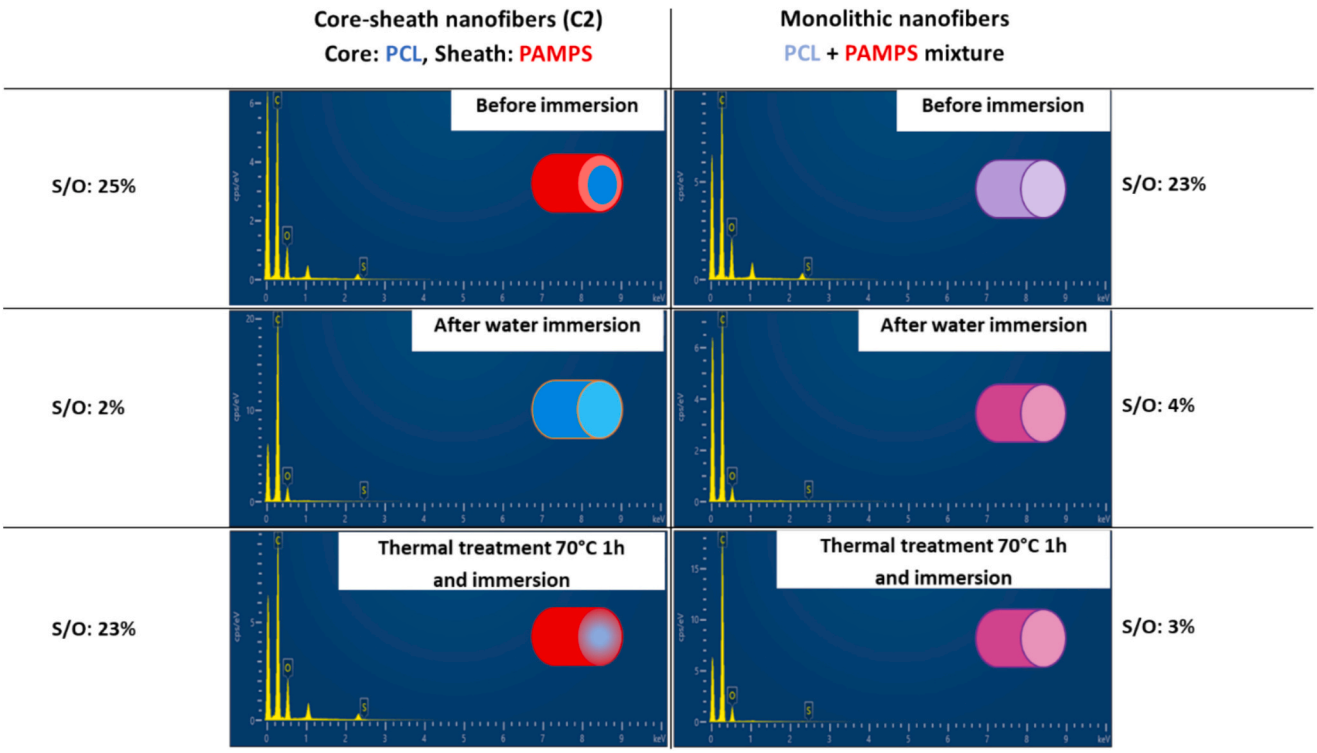

Fig. 5. Evaluation of the sulfur amount by EDX of core-sheath and monolithic nanofibrous membranes before and after immersion, and after thermal treatment at 70 °C for 1 h followed by an immersion in water. The sulfur amount is given in percentage in relation to a total ratio sulfur + oxygen. On each spectrum a scheme of the proposed nanofiber structure is presented.

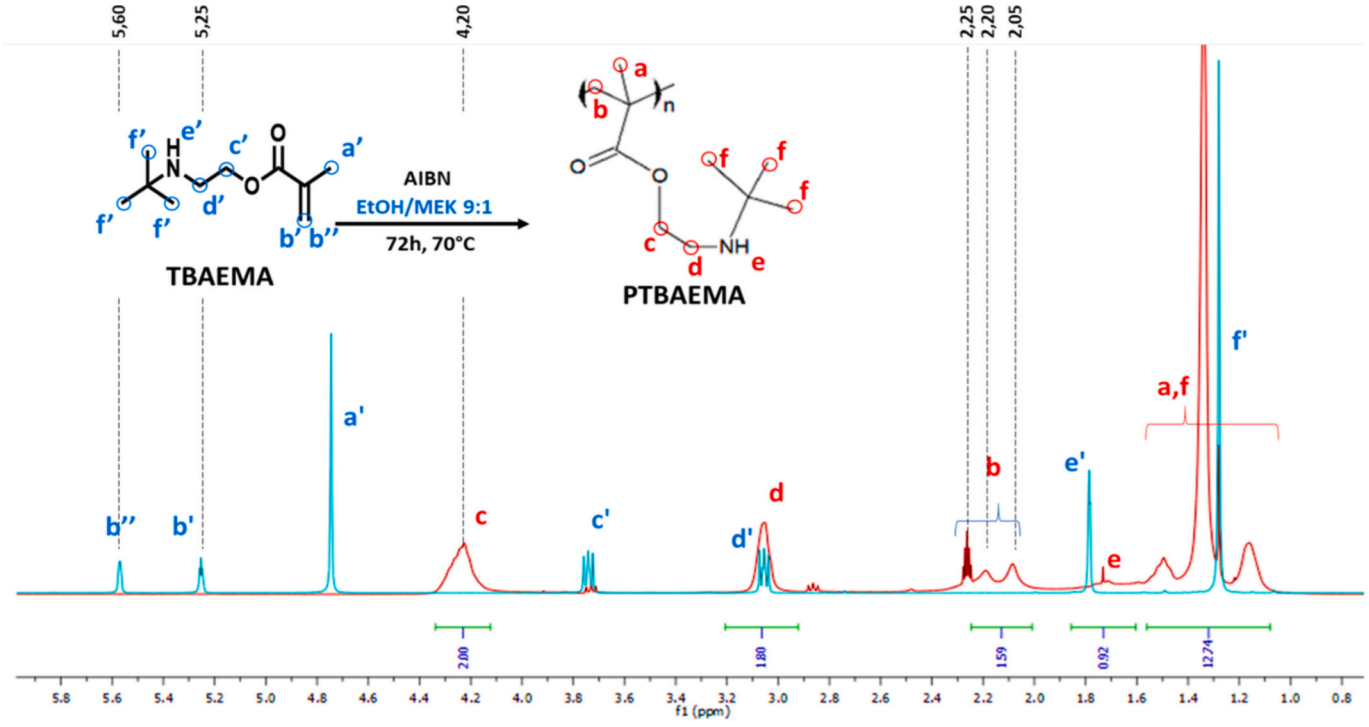

Fig. 6. ^{1}H NMR spectra of TBAEMA (blue) and PTBAEMA (red). (For interpretation of the references to color in this figure legend, the reader is referred to the web version of this article.)

or 25 wt% with DMFAe 5/5, it was not possible to obtained nanofibers. Moreover, for the other solvents with 14 wt% and 25 wt%, the obtained nanofibers exhibit numerous defaults such as high diameter dispersity or partially dissolved fibers (lack of solvent evaporation) as well as presence of some brittle nanofibers. By focusing on concentrations of 16 and 18 wt%, nanofibers presented a homogeneous diameter (between 100 and 300 nm) for each solvent except for Dac 5/5. For the two other mixtures, the optimal concentration was about 18 wt% for which

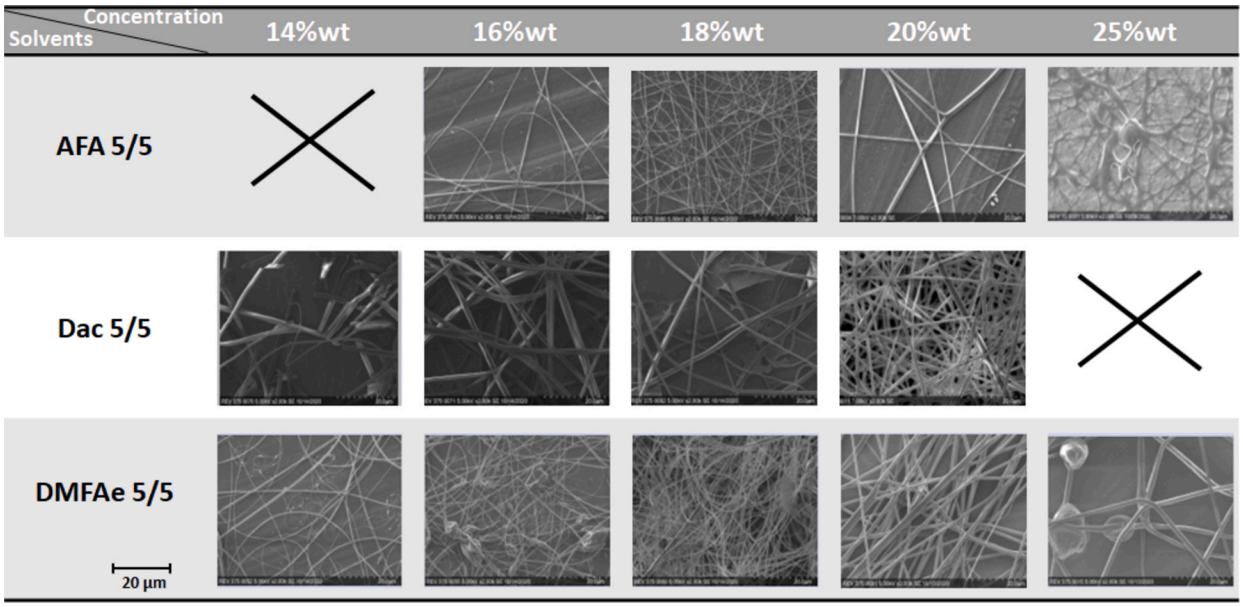

Fig. 7. SEM images of PTBAEMA nanofibers obtained from different electrospinning conditions.

homogeneous diameters of 247 ± 47 nm, and 152 ± 39 nm were obtained for AFA 5/5 and DMFAe 5/5, respectively.

The other electrospinning parameters were also varied, namely tip-to-collector distance and flow rate. The presence of defaults (beads and inhomogeneous diameters) was important for each modification. Thus, the optimal parameters of simple electrospinning of PTBAEMA were a tip-to-collector distance of 20 cm, a flow rate of 0.5 mL•h^{-1}, and a concentration of PTBAEMA of 18 wt% in mixture AFA 5/5 or DMFAe 5/5.

It also has to be mentioned that PTBAEMA powder as well as PTBAEMA nanofibers are insoluble in water.

3.3.2.2. Coaxial electrospinning of PCL/PTBAEMA. Coaxial electrospinning of PCL/PTBAEMA was performed, with an inner solution of 12 wt% of PCL in AFA 5/5 (as for PCL/PAMPS coaxial electrospinning) and an outer solution containing 18 wt% of PTBAEMA in AFA 5/5 or DMFAe 5/5 onto a PP mesh fixed on a rotating collector. Several couples of flow rates were tested: 0.2/0.4 mL•h^{-1}; 0.4/0.2 mL•h^{-1} and 0.2/0.2 mL•h^{-1} for core/sheath solutions. No nanofibrous structure could be obtained for the couple 0.2/0.2 mL•h^{-1} for each solvent mixture. Nevertheless, nanofibers with different morphologies were observed for the two other flow rates couples (Fig. 8A).

Results showed that for the couple of flow rate 0.4/0.2 mL•h^{-1}, it was not possible to obtain nanofibers with homogeneous diameters whatever the solvent mixture. Numerous solvent spots were also observed on the final membrane. However, for the couple of flow rates 0.2/0.4 mL•h^{-1}, nanofibers exhibited homogeneous diameters of 235 ± 80 nm for the mixture AFA 5/5, thanks to the compatibility of both solutions. On the contrary, for the mixture DMFAe 5/5, nanofibers with high diameter dispersity were obtained with an average diameter of 732 ± 253 nm. Thus, optimal parameters were 18 wt% of PTBAEMA in AFA 5/5 as sheath solution and 12 wt% of PCL in AFA 5/5 as core solution, with flow rates of 0.2/0.4 mL•h^{-1} (PCL/PTBAEMA). EDX analysis of core/sheath PCL/PTBAEMA nanofibers obtained in these optimal conditions allowed to highlight the presence of nitrogen in an amount of 4.3 (ratio N/O) in the nanofibrous mat (data not shown), which confirmed the presence of PTBAEMA in the final membrane.

TEM analysis was performed in order to evidence the coaxial structure of nanofibers obtained in these conditions (Fig. 8B). Results showed that some nanofibers present a difference of contrast between the core and the sheath. However, some nanofibers did not exhibit this phenomenon. This observation could be explained by the slight difference in chemical structure between PTBAEMA and PCL which implies a slight difference of density and therefore difficulties to observe a difference of

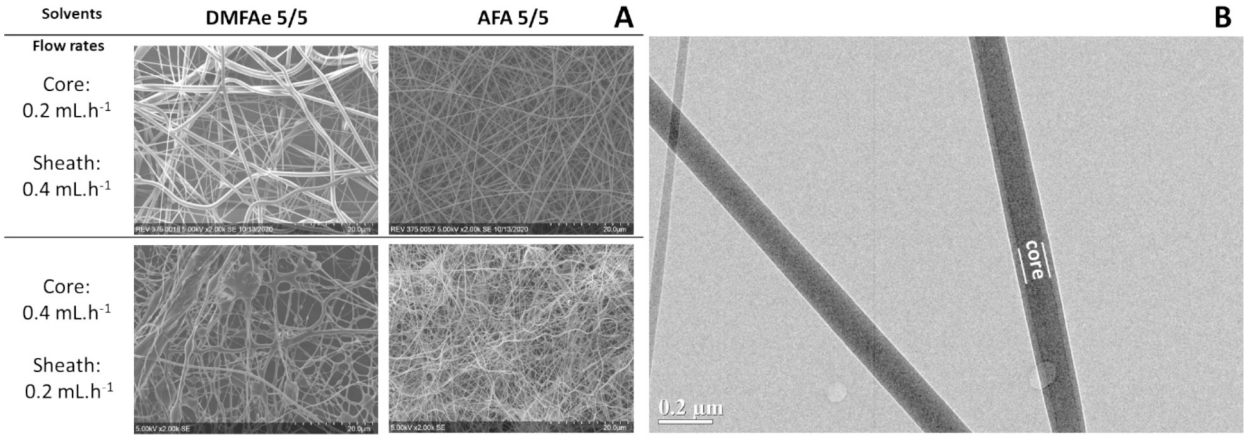

Fig. 8. A) PCL/PTBAEMA core-sheath nanofibers morphology obtained in different mixtures of solvents and with different couples of flow rates and B) TEM image of PCL/PTBAEMA core-sheath nanofibers (flow rates of 0.2/0.4).

contrast between the two phases of the fibers (core and sheath). Thus, it was difficult to conclude on the coaxial structure of the PCL/PTBAEMA nanofibers with this technique.

The PCL/PTBAEMA core-sheath nanofibers did not show any weight loss after 30 min immersion in water. EDX analysis showed the same proportion of N/O for immersed and non-immersed nanofibers confirming that there is no dissolution of the PTBAEMA sheath in water, as expected due to the insolubility of PTBAEMA in water. WCA analysis did not show any difference between the mixture of PCL and PTBAEMA and PCL/PTBAEMA core-sheath nanofibers with a contact angle about 90°, in accordance with the hydrophobicity of both PCL and PTBAEMA.

3.4. *In vitro* biological evaluation

In vitro biological assays were performed on gamma-sterilized PP meshes covered with core-sheath nanofibers obtained from coaxial electrospinning, and with monolithic nanofibers obtained from simple electrospinning of the mixtures of PCL and the bioactive polymers.

3.4.1. *Cytocompatibility assays*

Cytocompatibility was carried out on each series of core-sheath and monolithic nanofibers after 3 and 6 days of direct contact with NIH/3T3 cells (Fig. 9). The cell viability of PP mesh and PCL nanofibers was assessed in a previous paper and did not show any cytotoxicity [30].

PCL/PAMPS monolithic and core-sheath membranes show a cell proliferation of 29 % and 28 % after 3 days respectively. After 6 days, these proliferation rates increase slightly up to 35 % and 46 % for monolithic and core-sheath nanofibers respectively, indicating that the cytocompatibility is limited but delayed. In the case of PCL/PTBAEMA nanofibers, both monolithic and core-sheath membranes did not any show proliferation rates after 3 and 6 days, which can be explained by the toxicity of the antibacterial compound.

3.4.2. *Coagulation assays*

Coagulation assays were carried out on monolithic and core-sheath nanofibers based on PAMPS and compared to blood with or without heparin (Fig. 10). Pure PCL nanofibers were tested as control and did not show any increase of aPTT compared to blood [30]. For PAMPS-based nanofibrous membranes, the results are similar whatever the electrospinning method. Indeed, the presence of PAMPS-based nanofibers leads to a prolongation of aPTT from 86.9 s to >220 s compared to the gold standard heparin. A prolongation of PT from 18.1 s to 88.8 s (extrinsic pathway) compared to blood containing heparin is also observed. Although these results show no significant difference between core-sheath and monolithic PCL/PAMPS nanofibers, the anticoagulant activity observed in the case of monolithic nanofibers is probably due to

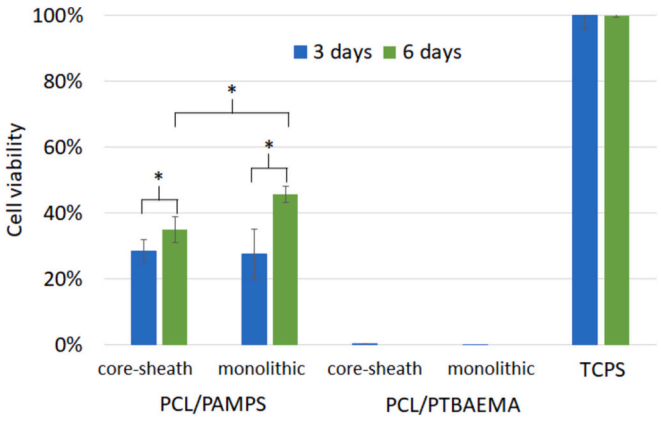

Fig. 9. NIH/3T3 cells viability after 3 and 6 days of contact with TCPS (control), PCL/PAMPS (thermally treated) and PCL/PTBAEMA core-sheath (coaxial) nanofibers and monolithic (mixture) nanofibers. *$p < 0.05$.

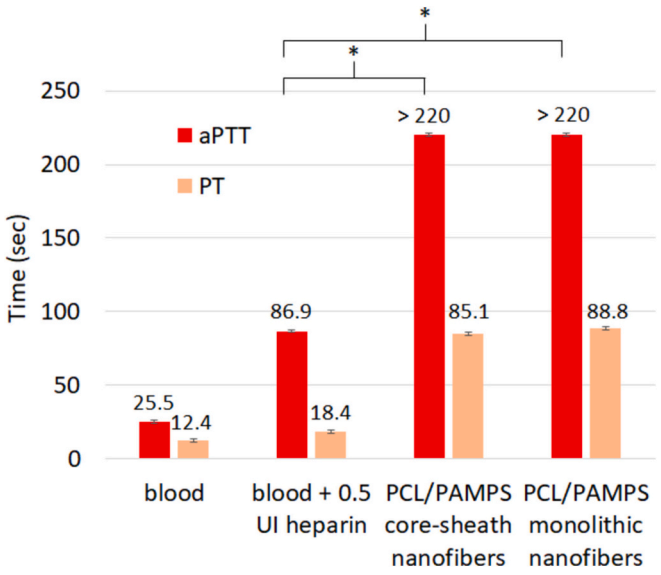

Fig. 10. Values of aPTT and PT of thermally treated PAMPS-based core-sheath and monolithic nanofibers compared to blood and blood containing 0.5UI heparin *$p < 0.05$.

the release of PAMPS in the medium during the test (according to S/O values determined by EDX after immersion values shown on Fig. 5). In these conditions, the anticoagulant activity of monolithic nanofibers should be observed in a shorter period compared to core-sheath nanofibers. These results show the heparin-like activity of PAMPS with similar mechanisms on the intrinsic pathway (aPTT) and on the extrinsic and common pathways (PT) of the coagulation cascade. On the contrary, the anti-Xa values are similar to that of fresh blood (<0.10 UI/mL) and lower than that obtained with blood containing heparin (1.51 ± 0.29 UI/mL), indicating that the PAMPS does not affect the inhibition of activated factor X by antithrombin.

3.4.3. *Antibacterial activity analysis*

Antibacterial activity of the PTBAEMA-based nanofibrous implants was assessed through kill time assay against *S. aureus* and *E. coli*. The results presented on Fig. 11 show that all the nanofibrous implants containing PTBAEMA exhibit a strong antibacterial effect against both Gram + and Gram − strains, with a higher affinity towards *S. aureus*. The antibacterial effect is maintained within 24 h. The monolithic nanofibers prepared by mixture of PCL and PTBAEMA present a high dispersion of the bacterial inhibition probably due to the bulk distribution of active groups within the nanofibers, whereas in the case of core-sheath nanofibers, the functional antibacterial groups are concentrated at the surface of the nanofibers. As expected, membranes based on PAMPS did not exhibit any antibacterial activity.

4. Discussion

The surgical treatment of abdominal hernia usually consists in the deposition of a mesh which plays the role of a mechanical barrier, reinforcing the abdominal wall and preventing the recurrence of this pathology. However, in more than half cases, two postoperative reactions may occur and are mainly located on two distinct contact areas. Indeed, the postoperative adhesions mainly occur at the interface between the peritoneal wall and the implant [13], whereas the infection risk is increased at the interface of the implant and the abdominal wall. According to clinical studies, commercial synthetic composite meshes designed for the prevention of postoperative adhesions are usually not recommended in contaminated areas, some studies showing an increase of infection occurrence and recurrence rates [13]. In the case of infected areas, biological meshes (allografts and xenograft tissues) rich in

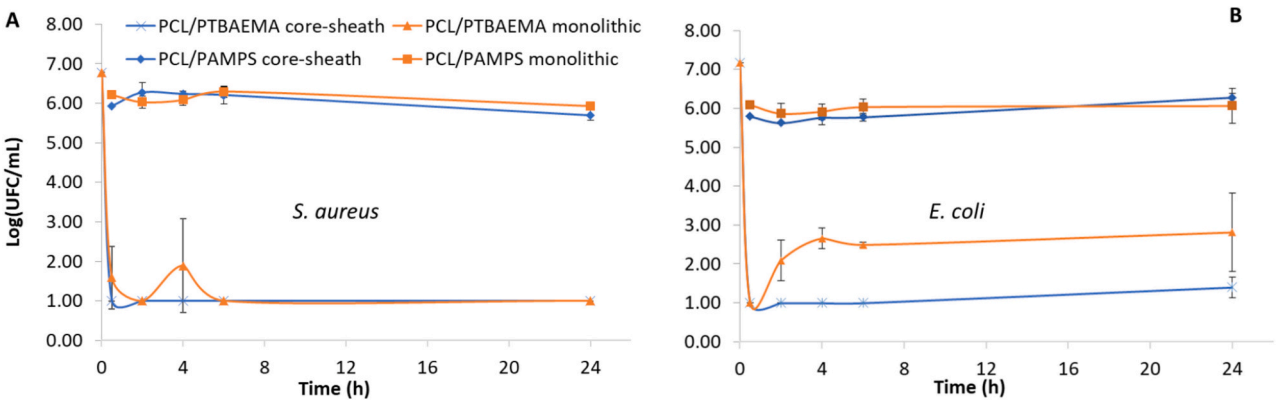

Fig. 11. Antibacterial activity of PCL/PTBAEMA and PCL/PAMPS core-sheath and monolithic nanofibers evaluated by kill-time assay against A) *S. aureus* and B) *E. coli* strains.

collagen can be used, but they have a higher cost and degrade faster compared to synthetic meshes [14]. Although the advantages and disadvantages of each mesh category are well identified, the choice and therefore the possible outcomes of the best material mesh among the multiple available solutions for a specific abdominal wall repair procedure finally depends mainly of the experience and knowledge of the surgeon [13]. In this context, our strategy consisted in functionalizing each face of the PP abdominal implant with a different bioactive polymer in order to prevent *in situ* both postoperative risks. For that purpose, impregnation of the implant in the functional polymers could not be considered: it would result in a coating of each PP fiber with both polymers on each face and therefore a reduction of the bioactivity towards the targeted surface. Moreover, the incompatibility of bioactive polymers could lead to a phase separation in the impregnation solution and therefore one polymer could be grafted at the expense of the other. In this application, the tissue integration of the mesh is of first importance to ensure proper healing of the damaged tissues and prevent mesh rejection by the body. In the literature, PP meshes coated with PCL electrospun nanofibers showed *in vivo* mechanical stability and similar tissue integration to uncoated PP meshes, with efficient vascularization [33]. These promising results were attributed to the porous nanostructure mimicking the extracellular one, promoting cell penetration, attachment and proliferation. The electrospinning technique was then chosen to design nanofibrous bioactive membranes that would be deposited separately on each face of the implant, which allows the use of a different bioactive polymer on each face of the PPM. On the contrary to the solutions used in surgery (peritoneal instillation, hydrogels), it would not require an additional step that could increase surgery time and therefore increase risks of contaminations. It also leads to a complete obstruction of the large pores of the PPM, which is expected to reduce the risks of diffusion of bacteria or the colonization of fibrin through the implant between peritoneal and abdominal walls. Moreover, the areas of contact between the two nanofibrous layers through the holes of the PP mesh improve the adhesion of these membranes to the mesh. The electrospinning process allows to design, from a wide range of synthetic polymers, nanofibrous membranes which exhibit large surface areas for an improved contact surface and expected improved bioactivity.

Different pathways were considered concerning the composition and structure of the nanofibrous layers: the simple electrospinning of the bioactive polymer, the coaxial electrospinning of PCL as core solution and the bioactive polymer as sheath solution, and finally, as presented in our previous paper, the simple electrospinning of PCL onto the mesh followed by cold-plasma induced graft copolymerization with the bioactive monomer [30]. The coaxial electrospinning presents the advantage to be a one step process for the formation of the functional coating, on the contrary to cold plasma induced grafting and other strategies from the literature [25,27].

Regarding the anti-adhesive activity, it is difficult to determine precisely the required bioactivity as adhesions result from a combination of factors. However, adhesions result from an excessive production of fibrin, which is formed through the coagulation cascade. We hypothesized that an anticoagulant activity could reduce the amount of fibrin and prevent its persistence. As heparin is the gold standard for anticoagulant activity, we selected PAMPS as heparin-like polymer possessing sulfonic acid groups [34]. In particular, the corresponding monomer AMPS can be polymerized by radical polymerization in solution or through cold-plasma induced polymerization process. As PAMPS is soluble in water, the obtained pure PAMPS nanofibrous monolithic membranes did not exhibit sufficient stability in water for the application. However, the coaxial electrospinning of PCL/PAMPS solutions followed by a thermal treatment allowed to obtain biodegradable nanofibrous membranes with improved stability in water, while maintaining PAMPS at the surface and *in vitro* anticoagulant activity with heparin-like properties. In our previous study, we successfully developed PPM-PCL membranes grafted with AMPS through cold plasma induced graft copolymerization [30]. These devices presented lower *in vitro* anticoagulant activity (aPTT values close to the blood containing heparin ones). However, the samples exhibited a similar behavior in terms of delayed cell viability between 3 and 6 days, but with a better cytocompability of around 55 % after 6 days. Moreover, these membranes did not require any thermal post-treatment. Therefore, by taking into account the cytocompatibility, cold-plasma grafted PAMPS nanofibers perform better than the core-sheath nanofibers.

Concerning the antibacterial activity, we chose a polymer bearing a polar tertiary amine, known for its bacteria membrane-damaging properties [24,35]. The coaxial electrospinning of PCL and PTBAEMA solutions led to the formation of nanofibers which core-sheath structure was hardly observed due to the similar densities of the polymers. The presence of PCL as core helped improving the formation of smooth nanofibers. No additional thermal treatment was necessary thanks to the insolubility of PTBAEMA in water. The presence of a high amount of antibacterial groups at the surface was confirmed by the strong cytotoxicity of the membranes and the prolonged antibacterial effect against the tested Gram+ and Gram- strains. In particular, the core-sheath structure proved to enhance the antibacterial activity in terms of efficacy and reproducibility compared to monolithic one, thanks to a concentration of the functional groups in the outer layer of the nanofibers. It is important to note that, despite numerous attempts varying the solution and cold plasma parameters, the cold-plasma induced graft copolymerization of TBAEMA onto PCL nanofibers could not be achieved, probably due to the low reactivity of TBAEMA in these conditions.

Therefore, considering the results presented in this paper and compared to our previous study, the optimal design of a bifacial PP

abdominal mesh for the prevention of both postoperative adhesions and infections would be as follows: one face covered by PCL nanofibers grafted with PAMPS thanks to cold plasma induced polymerization for anticoagulant activity and one face covered by PCL/PTBAEMA core-sheath nanofibers for antibacterial activity.

These promising results show the great potential of these new composite materials for *in vivo* evaluation of postoperative adhesions and infections. The literature concerning the development of PP meshes covered with PCL electrospun nanofibers and their evaluation showed suitable biomechanical properties, good tissue integration and vascularization [33]. In our case, *in vivo* assays will also evaluate the impact of the anticoagulant PAMPS and antimicrobial PTBAEMA coatings on the tissue integration of the composite meshes and their *in situ* activity towards fibrin formation and infections. Moreover, these assays will also determine the *in vivo* degradation of the membranes, which could further be adjusted by simply replacing the core bioresorbable polymer, using polylactic acid (PLA) or poly(lactic-*co*-glycolic acid) (PLGA) for example instead of PCL. Indeed, fibrin formation occur within the first seven days after surgery whereas infections may occur within a month after implantation. The use of a short-term bioresorbable polymer could therefore be sufficient, but the choice of this polymer would be carefully driven by the balance between resorption and tissue integration. This study would allow to compare the advantages and limitations of our composite meshes with the other strategies from the literature and commercial solutions.

5. Conclusions

The aim of this project was to cover PP meshes with nanofibrous layers based on a biodegradable polymer (PCL) and bioactive polymers (PAMPS and PTBAEMA). The role of biodegradable PCL is to be degraded in the organism leaving in place the PP implant, which is necessary to maintain a mechanical barrier preventing the recurrence of hernia, once the therapeutic activity would be achieved. The bioactive polymers were selected in order to provide anticoagulant (PAMPS) or antibacterial (PTBAEMA) activity to the meshes. Coaxial electrospinning was successfully used to form core/sheath fibers with PCL as core and PAMPS or PTBAEMA as sheath, which structure was confirmed by TEM in the case of PCL/PAMPS nanofibers, which had to be thermally post-treated to enhance their stability in water. The core-sheath structure of PCL/PTBAEMA nanofibers was not clearly evidenced by TEM, however the nanofibers did not require any further treatment to improve their stability in water. *In vitro* anticoagulant assays showed an important increase of the coagulation time for PCL/PAMPS core-sheath nanofibers, whereas antibacterial assays clearly demonstrated the antibacterial activity of PCL/PTBAEMA core-sheath nanofibers.

The process presented in this paper allows to easily cover separately each side of the PP mesh. The choice of the biodegradable core polymer could be easily tuned in order to aim a specific degradation rate. Indeed, the promising *in vitro* bioactivity results open the door to the development of a bifacial abdominal implant, whose each side would exhibit a different bioactivity adapted to the surrounding tissue once implanted by the surgeon. More specifically, the anticoagulant surface would be active towards the peritoneal wall to prevent adhesions, whereas the antibacterial surface would be active towards the visceral wall to prevent infections. Up to now, such an abdominal active implant does not exist and would be of great interest to prevent postoperative risks after hernia surgery.

CRediT authorship contribution statement

Malo Dufay: Writing – original draft, Methodology, Investigation, Formal analysis. **Maude Jimenez:** Writing – review & editing, Validation, Supervision, Methodology, Conceptualization. **Mathilde Casetta:** Methodology. **Feng Chai:** Methodology, Investigation. **Nicolas Blanchemain:** Writing – review & editing, Methodology. **Mickael Maton:** Methodology, Investigation. **Frédéric Cazaux:** Methodology. **Séverine Bellayer:** Methodology. **Stéphanie Degoutin:** Writing – review & editing, Writing – original draft, Supervision, Project administration, Investigation, Funding acquisition, Data curation, Conceptualization.

Declaration of competing interest

The authors declare the following financial interests/personal relationships which may be considered as potential competing interests:

DEGOUTIN Stephanie reports financial support was provided by University of Lille Faculty of Science and Technology. If there are other authors, they declare that they have no known competing financial interests or personal relationships that could have appeared to influence the work reported in this paper.

Acknowledgments

The authors thank Agence Nationale de la Recherche (ANR JCJC CAPSPIN: ANR-17-CE09-0003-01) and Euramaterials competitiveness Cluster for supporting and funding this work. Thanks to Alexandre Ung (service Hémostase, Hospital Center University of Lille (CHU-Lille)) for help in blood coagulation test. The Chevreul Institute is thanked for its help in the development of this work through the ARCHI-CM project supported by the "Ministère de l'Enseignement Supérieur de la Recherche et de l'Innovation", the region "Hauts-de-France", the ERDF program of the European Union and the "Métropole Européenne de Lille".

Appendix A. Supplementary data

Supplementary data to this article can be found online at https://doi.org/10.1016/j.bioadv.2024.214163.

Data availability

The data that has been used is confidential.

References

[1] A. Kingsnorth, K. LeBlanc, Hernias: inguinal and incisional, Lancet 362 (9395) (2003) 1561–1571.
[2] W.B. Gaertner, M.E. Bonsack, J.P. Delaney, Visceral adhesions to hernia prostheses, Hernia 14 (4) (2010) 375–381.
[3] S. Muniredy, S.L. Kavalukas, A. Barbul, Intra-abdominal healing: gastrointestinal tract and adhesions, Surg. Clin. N. Am. 90 (6) (2010) 1227–1236.
[4] R. Rosch, M. Binnebösel, K. Junge, P. Lynen-Jansen, P.R. Mertens, U. Klinge, V. Schumpelick, The instable scar, in: V. Schumpelick, R.J. Fitzgibbons (Eds.), Recurrent Hernia: Prevention and Treatment, Springer Berlin Heidelberg, Berlin, Heidelberg, 2007, pp. 59–62.
[5] M.E. Falagas, S.K. Kasiakou, Mesh-related infections after hernia repair surgery, Clin. Microbiol. Infect. 11 (1) (2005) 3–8.
[6] I. Vassiliou, A. Tympa, T. Theodosopoulos, C. Nastos, N. Arkadopoulos, N. Dafnios, G. Fragulidis, E. Kouskouni, V. Smyrniotis, Late polypropylene mesh susceptibility to infection during intra-abdominal sepsis, J. Invest. Surg. 24 (5) (2011) 199–204.
[7] T. Saha, X. Wang, R. Padhye, S. Houshyar, A review of recent developments of polypropylene surgical mesh for hernia repair, OpenNano 7 (2022) 100046.
[8] A. Fatehi Hassanabad, A.N. Zarzycki, K. Jeon, J.A. Dundas, V. Vasanthan, J. F. Deniset, P.W.M. Fedak, Prevention of post-operative adhesions: a comprehensive review of present and emerging strategies, Biomolecules 11 (7) (2021).
[9] G. Guzmán-Valdivia Gómez, E. Tena-Betancourt, M. Angulo Trejo, Different doses of enoxaparin in the prevention of postoperative abdominal adhesions. Experimental study, Ann. Med. Surg. 73 (103132) (2021).
[10] C.B. Brown, A.A. Luciano, D. Martin, E. Peers, A. Scrimgeour, G.S. diZerega, Adept (icodextrin 4% solution) reduces adhesions after laparoscopic surgery for adhesiolysis: a double-blind, randomized, controlled study, Fertil. Steril. 88 (5) (2007) 1413–1426.
[11] L. Mettler, A. Audebert, E. Lehmann-Willenbrock, K. Schive, V.R. Jacobs, Prospective clinical trial of SprayGel as a barrier to adhesion formation: an interim analysis, J. Am. Assoc. Gynecol. Laparosc. 10 (3) (2003) 339–344.
[12] M.L. Baptista, M.E. Bonsack, J.P. Delaney, Seprafilm reduces adhesions to polypropylene mesh, Surgery 128 (1) (2000) 86–92.
[13] A. Costa, S. Adamo, F. Gossetti, L. D'Amore, F. Ceci, P. Negro, P. Bruzzone, Biological scaffolds for abdominal wall repair: future in clinical application? Materials 12 (15) (2019) 2375.

[14] A. Najm, A.-G. Niculescu, B.S. Gaspar, A.M. Grumezescu, M. Beuran, A review of abdominal meshes for hernia repair—current status and emerging solutions, Materials 16 (22) (2023) 7124.
[15] O. Guillaume, R. Pérez-Tanoira, R. Fortelny, H. Redl, T.F. Moriarty, R.G. Richards, D. Eglin, A. Petter Puchner, Infections associated with mesh repairs of abdominal wall hernias: are antimicrobial biomaterials the longed-for solution? Biomaterials 167 (2018) 15–31.
[16] S. Mirel, A. Pusta, M. Moldovan, S. Moldovan, Antimicrobial meshes for hernia repair: current progress and perspectives, J. Clin. Med. 11 (3) (2022).
[17] F. Corduas, D.A. Lamprou, E. Mancuso, Next-generation surgical meshes for drug delivery and tissue engineering applications: materials, design and emerging manufacturing technologies, Bio-Des. Manuf. 4 (2) (2021) 278–310.
[18] D. Wei, Y. Huang, M. Liang, P. Ren, Y. Tao, L. Xu, T. Zhang, Z. Ji, Q. Zhang, Polypropylene composite hernia mesh with anti-adhesion layer composed of PVA hydrogel and liposomes drug delivery system, Colloids Surf. B Biointerfaces 223 (2023) 113159.
[19] A. Muñoz-Bonilla, M. Fernández-García, Polymeric materials with antimicrobial activity, Prog. Polym. Sci. 37 (2) (2012) 281–339.
[20] J.C. Tiller, C.J. Liao, K. Lewis, A.M. Klibanov, Designing surfaces that kill bacteria on contact, Proc. Natl. Acad. Sci. U. S. A. 98 (11) (2001) 5981–5985.
[21] T. Ravikumar, H. Murata, R.R. Koepsel, A.J. Russell, Surface-active antifungal polyquaternary amine, Biomacromolecules 7 (10) (2006) 2762–2769.
[22] Y. Wang, Y. Tang, Z. Zhou, E. Ji, G.P. Lopez, E.Y. Chi, K.S. Schanze, D.G. Whitten, Membrane perturbation activity of cationic phenylene ethynylene oligomers and polymers: selectivity against model bacterial and mammalian membranes, Langmuir 26 (15) (2010) 12509–12514.
[23] E.R. Kenawy, F.I. Abdel-Hay, A.E.-R.R. El-Shanshoury, M.H. El-Newehy, Biologically active polymers. V. Synthesis and antimicrobial activity of modified poly(glycidyl methacrylate-co-2-hydroxyethyl methacrylate) derivatives with quaternary ammonium and phosphonium salts, J. Polym. Sci. Pt. A 40 (2002) 2384–2393.
[24] J.-M. Thomassin, S. Lenoir, J. Riga, R. Jérôme, C. Detrembleur, Grafting of poly[2-(tert-butylamino)ethyl methacrylate] onto polypropylene by reactive blending and antibacterial activity of the copolymer, Biomacromolecules 8 (4) (2007) 1171–1177.
[25] Q. Saiding, Y. Chen, J. Wang, C.L. Pereira, B. Sarmento, W. Cui, X. Chen, Abdominal wall hernia repair: from prosthetic meshes to smart materials, Mater. Today Bio 21 (2023) 100691.
[26] M. Plencner, E. Prosecká, M. Rampichová, B. East, M. Buzgo, L. Vysloužilová, J. Hoch, E. Amler, Significant improvement of biocompatibility of polypropylene mesh for incisional hernia repair by using poly-ε-caprolactone nanofibers functionalized with thrombocyte-rich solution, Int. J. Nanomedicine 10 (2015) 2635–2646.
[27] Y. Mao, Y. Meng, S. Li, Y. Li, R. Guidoin, F. Wang, Y. Qiao, G. Brochu, Z. Zhang, J. Tang, L. Wang, Alginate-assistant nanofiber integrated with polypropylene hernia mesh for efficient anti-adhesion effects and enhanced tissue compatibility, Compos. Part B Eng. 235 (2022) 109761.
[28] Z. Zhang, L. Zhu, W. Hu, J. Dai, P. Ren, X. Shao, B. Xiong, T. Zhang, Z. Ji, Polypropylene mesh combined with electrospun poly (L-lactic acid) membrane in situ releasing sirolimus and its anti-adhesion efficiency in rat hernia repair, Colloids Surf. B Biointerfaces 218 (2022) 112772.
[29] M. Dufay, M. Jimenez, S. Degoutin, Effect of cold plasma treatment on electrospun nanofibers properties: a review, ACS Appl. Bio Mater. 3 (8) (2020) 4696–4716.
[30] M. Dufay, M. Jimenez, M. Casetta, F. Chai, N. Blanchemain, G. Stoclet, F. Cazaux, S. Bellayer, S. Degoutin, PCL covered PP meshes plasma-grafted by sulfonated monomer for the prevention of postoperative abdominal adhesions, Mater. Today Commun. 26 (2021) 101968.
[31] L.W. Fisher, A.R. Sochor, J.S. Tan, Chain characteristics of poly(2-acrylamido-2-methylpropanesulfonate) polymers. 1. Light-scattering and intrinsic-viscosity studies, Macromolecules 10 (5) (1977) 949–954.
[32] F. Sosna, P. Ottersbach, B. Kossmann, Antimicrobial Additives, USA, 2004.
[33] M. Plencner, B. East, Z. Tonar, M. Otáhal, E. Prosecká, M. Rampichová, T. Krejčí, A. Litvinec, M. Buzgo, A. Míčková, A. Nečas, J. Hoch, E. Amler, Abdominal closure reinforcement by using polypropylene mesh functionalized with poly-ε-caprolactone nanofibers and growth factors for prevention of incisional hernia formation, Int. J. Nanomedicine 9 (2014) 3263–3277.
[34] S.J. Paluck, T.H. Nguyen, H.D. Maynard, Heparin-mimicking polymers: synthesis and biological applications, Biomacromolecules 17 (11) (2016) 3417–3440.
[35] M. Pakhira, S. Ghosh, S. Ghosh, D.P. Chatterjee, A.K. Nandi, Development of poly (vinylidene fluoride) graft random copolymer membrane for antifouling and antimicrobial applications, J. Ind. Eng. Chem. 112 (2022) 171–181.